2010 IEEE International Conference on Robotics and Automation
Anchorage Convention District
May 3-8, 2010, Anchorage, Alaska, USA

Terramechanics-based High-Fidelity Dynamics Simulation for Wheeled Mobile Robot on Deformable Rough Terrain

Liang Ding, Keiji Nagatani, Keisuke Sato, Andres Mora, Kazuya Yoshida, Haibo Gao, Zongquan Deng

Abstract—**Numerical simulation analysis of the motion of wheeled mobile robots is significant for both their R&D and control phases, especially due to the recent increase in the number of planetary exploration missions. Using the position/orientation of the rover body and all the joint angles as generalized coordinates, the Jacobian matrices and recursive dynamic models are derived. Terramechanics models for calculating the forces and moments that act on the wheel—as a result of the deformable soil—are introduced in consideration of the effect of normal force. A rough terrain modeling method is developed for estimating the wheel-soil interaction area, wheel sinkage, and the terminal coordinate. A simulation program that includes the above techniques is developed using Matlab and SpaceDyn Toolbox. Experimental results from a 4-wheeled mobile robot moving on Toyoura soft sand are used to verify the fidelity of the simulation. A simulation example of a robot moving on a random rough terrain is also presented.**

I. Introduction

The Sojourner rover and Mars Exploration Rovers (MER) have proven the effectiveness of wheeled mobile robots (WMRs) in planetary exploration missions. Future missions will require the robots to traverse over more challenging deformable rough terrain.

Dynamic simulation plays an important role in both the R&D and tele-operation phases of WMRs [1]. During the R&D phase of a WMR, dynamic simulation can be used for mechanical design/evaluation/optimization, mobility performance analysis, control strategy validation, etc. While for the operation phase, dynamic simulation can be used to support 3D predictive displays for successive tele-operation (such as a lunar rover) or to validate command sequences for the supervised tele-operation (such as a Mars rover).

The dynamics of WMRs is primarily composed of two parts: the multi-rigid-body dynamics of the vehicle and the wheel-soil interaction terramechanics, which is intricate but important for improving the fidelity of a simulation. Some dynamic simulation platforms have been developed on the basis of conventional terrestrial vehicle terramechanics. NASA's Jet Propulsion Laboratory (JPL) developed the Rover Analysis, Modeling and Simulation (ROAMS) system for real-time simulation of planetary rovers [2-3], which uses a single degree-of-freedom Hunt-Crossley compliance system at each wheel to compute the force in the normal direction; and a two degree-of-freedom compliance system to compute tangent forces with a linear spring-damper model [4]. Based on Bekker's classical terramechanics theory, a computational framework—Locomotion Synthesis (LocSyn)—for mobile robots was developed by combining a simulation of the performance prediction and the optimization of configuration parameters [5]. A set of tools has been developed by the ESA named RCET (Rover Chassis Evaluation Tools) to support the design, selection, and optimization of space exploration rovers. The tools consist of a tractive prediction module that deals with the wheel-terrain interaction based on Bekker's traditional terramechanics theory [6]. The Rover Performance Evaluation Tool (RPET) is a systematic tool, developed by the Surrey Space Center and DLR, for evaluating the rover chassis through the application of Bekker's theory [7]. RCAST combines a rigid multi-body dynamics engine available in Matlab with the AS^{2}TM wheel-soil interaction module, and it was developed to optimize the ExoMars Rover mobility for the evaluation of locomotion subsystem designs [8].

Due to the differences between WMRs and terrestrial vehicles in terms of physical dimension, wheel shape, payload, terrain, running velocity, and control mode, etc., it is necessary to examine the applicability of conventional terramechanics theory and to improve it by targeting WMRs. Yoshida et al. from the Space Robotics Laboratory (SRL) at Tohoku university have been researching terramechanics for planetary exploration robots [9]. The conventional Wong-Reece terramechanics formula was employed to derive an improved practical model for calculating drawbar pull [10]. In order to analyze the steering performance of a wheel and a rover, the lateral force of a driving wheel was modeled [11]. Based on the results of research into terramechanics models, Ishigami et al. built an all-wheel dynamics model and analyzed the motion dynamics for wheeled robots [12]. The virtual simulation platform was then used for motion analysis, control strategy verification, and path evaluation [13].

This study greatly improves the fidelity of the simulation platform developed at SRL by embedding high-fidelity terramechanics models and dealing with the contact between deformable rough terrain and different wheels rather than an entire rover. A generalized dynamics model for mobile robots,

This work was supported by the National Natural Science Foundation of China (50975059), Key Natural Science Foundation of Heilongjiang Province in China (ZJG0709), Foundation of Chinese State Key Laboratory of Robotics and System (grant No. SKLRS200801A02), Key Laboratory Opening Funding of Aerospace Mechanism and Control (HIT. KLOF. 2009060) and "111" Project (B07018).

L. Ding, H. Gao, and Z. Deng, School of Mechatronics Engineering, Harbin Institute of Technology, Harbin 150001, Heilongjiang, China; State Key Laboratory of Robotics and System (HIT), Harbin 150001, Heilongjiang, China (e-mail: liang.ding@hotmail.com, {gaohaibo, dengzq}@hit.edu.cn).

K. Nagatani, K. Sato, A. Mora, K. Yoshida, and Liang Ding, Department of Aerospace Engineering, Tohoku University, Aoba 6-6-01, Sendai, 980-8579, Japan (e-mail: { keiji, keisuke, andresmora, yoshida, liangding} @astro.mech.tohoku.ac.jp).

considering all the external forces and moments that act on the wheels, is deduced in Section II. A high-fidelity driving terramechanics model considering wheel lug effect and slip-sinkage, as well as a steering model are introduced in Section III. Section IV describes the method for estimating the wheel-soil contact area on deformable soil. Section V presents the simulation implementation, experimental validation, and an example.

II. Generalized Recursive Dynamics Modeling

A. Recursive Kinematics and Jacobian Matrices

If $\boldsymbol{a}=[a_1 \quad a_2 \quad a_3]^T$, $\boldsymbol{b}=[b_1 \quad b_2 \quad b_3]^T$, define $\tilde{\boldsymbol{a}}=\begin{bmatrix} 0 & -a_3 & a_2 \\ a_3 & 0 & -a_1 \\ -a_2 & a_1 & 0 \end{bmatrix}$, then $\boldsymbol{a}\times\boldsymbol{b}=\tilde{\boldsymbol{a}}\boldsymbol{b}$, $\boldsymbol{b}\times\boldsymbol{a}=-\tilde{\boldsymbol{a}}\boldsymbol{b}=\tilde{\boldsymbol{a}}^T\boldsymbol{b}$.

Let $\boldsymbol{q}=[q_1 \quad q_2 \quad \cdots \quad q_{n_v}]^T$ denote the joint variables, where n_v is the number of joints. The WMRs are articulated multi-body systems with a moving base and n_w end-points (wheels). Let $\boldsymbol{q}_s=[q_l \quad q_m \quad q_n \quad \cdots \quad q_s]^T$ denote a branch from the rover body to a wheel, n_s denote the number of elements in $\boldsymbol{q}_s$. Replace the joint number l, m, n, …, s of the branch with 1, 2, 3, … , n_s, as shown in Fig. 1, which also shows the inertial coordinate $\{\Sigma_I\}$, and the coordinates $\{\Sigma_i\}$ attached to link i ($i = l, m, n, \ldots, s$) and related vectors, where $\boldsymbol{p}_i$ is the position vector of joint i; $\boldsymbol{r}_i$ is the position vector of the centroid of link i; $\boldsymbol{c}_{ij}$ is the link vector from link i to joint j; $\boldsymbol{l}_{ij} = \boldsymbol{p}_j - \boldsymbol{p}_i$ is the link vector from joint i to joint j; and $\boldsymbol{l}_{ie}$ is the vector from joint i to end-point e.

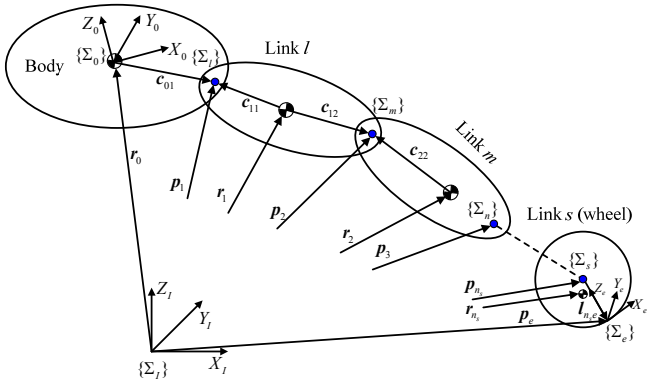

Fig. 1 Coordinates and vectors from rover body to a wheel

The position vector of end-point $\boldsymbol{p}_e$ is:

$$\boldsymbol{p}_e = \boldsymbol{r}_0 + \boldsymbol{c}_{01} + \sum_{i=1}^{n_s-1} \boldsymbol{l}_{i(i+1)} + \boldsymbol{l}_{n_s e} \tag{1}$$

The derivative of Eq. (1) is:

$$\begin{aligned} \boldsymbol{v}_e &= \boldsymbol{v}_0 + \boldsymbol{\omega}_0 \times (\boldsymbol{p}_e - \boldsymbol{r}_0) + \sum_{i=1}^{n_s} \boldsymbol{A}_i \, {}^i\boldsymbol{Z}_i \times (\boldsymbol{p}_e - \boldsymbol{p}_i)\dot{q}_i \\ &= \begin{bmatrix} \boldsymbol{J}_{BTe} & \boldsymbol{J}_{MTe} \end{bmatrix} \begin{bmatrix} \begin{pmatrix} \boldsymbol{v}_0^T & \boldsymbol{\omega}_0^T \end{pmatrix} & \dot{\boldsymbol{q}}^T \end{bmatrix}^T \end{aligned} \tag{2}$$

where $\boldsymbol{J}_{MTe} = [\boldsymbol{L}_{s1}\boldsymbol{A}_1 \, {}^1\boldsymbol{Z}_1 \times \boldsymbol{P}_{1e} \quad \boldsymbol{L}_{s2}\boldsymbol{A}_2 \, {}^2\boldsymbol{Z}_2 \times \boldsymbol{P}_{2e} \quad \cdots \quad \boldsymbol{L}_{sn_v}\boldsymbol{A}_{n_v} \, {}^{n_r}\boldsymbol{Z}_{n_v} \times \boldsymbol{P}_{n_v e}]$ is a $3\times n_v$ matrix, $\boldsymbol{A}_i = {}^I\boldsymbol{A}_i$ is the transformation matrix from $\{\Sigma_i\}$ to $\{\Sigma_I\}$[14], ${}^i\boldsymbol{Z}_i = [0 \quad 0 \quad 1]^T$, because the z axis is set to coincide with the joint displacement axis, $\boldsymbol{L}_{ij}$ is an element of matrix $\boldsymbol{L}_{n_v \times n_v}$ to indicate whether link j is on the access road from link 0 to link i ($\boldsymbol{L}_{ij}$=1) or not ($\boldsymbol{L}_{ij}$ = 0), $\boldsymbol{P}_{ie}$ is the vector from the origin of $\{\Sigma_i\}$ to the end point. $\boldsymbol{J}_{BTe} = [\boldsymbol{E} \quad \tilde{\boldsymbol{P}}_{er0}^T]$ is a 3×6 matrix, where $\boldsymbol{P}_{er0} = \boldsymbol{p}_e - \boldsymbol{r}_0$.

The angular velocity of the end-point is:

$$\boldsymbol{\omega}_e = \boldsymbol{\omega}_0 + \sum_{i=1}^{n_v} \boldsymbol{A}_i \, {}^i\boldsymbol{Z}_i \dot{q}_i = \begin{bmatrix} \boldsymbol{J}_{BRe} & \boldsymbol{J}_{MRe} \end{bmatrix} \begin{bmatrix} \begin{pmatrix} \boldsymbol{v}_0^T & \boldsymbol{\omega}_0^T \end{pmatrix} & \dot{\boldsymbol{q}}^T \end{bmatrix}^T \tag{3}$$

where $\boldsymbol{J}_{MRe} = [\boldsymbol{L}_{s1}\boldsymbol{A}_1 \, {}^1\boldsymbol{Z}_1 \quad \boldsymbol{L}_{s2}\boldsymbol{A}_2 \, {}^2\boldsymbol{Z}_2 \quad \cdots \quad \boldsymbol{L}_{sn_v}\boldsymbol{A}_{n_v} \, {}^{n_r}\boldsymbol{Z}_{n_v}]$ is a $3\times n_s$ matrix and $\boldsymbol{J}_{BRe} = [0 \quad \boldsymbol{E}]$ is a 3×6 matrix.

Let $\boldsymbol{J}_e = \begin{bmatrix} \boldsymbol{J}_{Be} & \boldsymbol{J}_{Me} \end{bmatrix} = \begin{bmatrix} \boldsymbol{J}_{BTe} & \boldsymbol{J}_{MTe} \\ \boldsymbol{J}_{BRe} & \boldsymbol{J}_{MRe} \end{bmatrix}$, be the $6\times(6+n_v)$ Jacobian matrix for mapping generalized velocities to the end-points; $\dot{\boldsymbol{\Phi}} = \begin{bmatrix} \begin{pmatrix} \boldsymbol{v}_0^T & \boldsymbol{\omega}_0^T \end{pmatrix} & \dot{\boldsymbol{q}}^T \end{bmatrix}^T$, a vector with $(6+n_v)$ elements, i.e., linear velocities and angular velocities of the body, and joint velocities. Let $\dot{\boldsymbol{X}}_{ae}$ and $\boldsymbol{J}_{ae}$ denote the velocities of all the wheel-soil interaction points and the corresponding Jacobian matrix:

$$\dot{\boldsymbol{X}}_{ae} = \begin{bmatrix} \boldsymbol{v}_e(1) \\ \boldsymbol{\omega}_e(1) \\ \vdots \\ \boldsymbol{v}_e(n_w) \\ \boldsymbol{\omega}_e(n_w) \end{bmatrix}, \quad \boldsymbol{J}_{ae} = \begin{bmatrix} \boldsymbol{J}_e(1) \\ \boldsymbol{J}_e(2) \\ \vdots \\ \boldsymbol{J}_e(n_w) \end{bmatrix},$$

the $6n_w \times 1$ vector and $6n_w \times (n_v + 6)$ matrix, respectively. The following is then obtained:

$$\dot{\boldsymbol{X}}_{ae} = \boldsymbol{J}_{ae}\dot{\boldsymbol{\Phi}} \tag{4}$$

The same method is used to deduce the Jacobian matrix by mapping the velocities from the generalized coordinates to the link centroid, and Eq. (5) is obtained:

$$\dot{\boldsymbol{X}}_a = \boldsymbol{J}_a\dot{\boldsymbol{\Phi}}, \tag{5}$$

where $\dot{\boldsymbol{X}}_a$ ($6n_v \times 1$) is the velocity vector of all the centroid, $\boldsymbol{J}_a$ ($6n_v \times (n_v + 6)$), the Jacobian matrix. In Eq. (5),

$$\dot{\boldsymbol{X}}_a = \begin{bmatrix} \boldsymbol{v}_1 \\ \boldsymbol{\omega}_1 \\ \vdots \\ \boldsymbol{v}_{n_v} \\ \boldsymbol{\omega}_{n_v} \end{bmatrix}, \quad \boldsymbol{J}_a = \begin{bmatrix} \boldsymbol{J}_1 \\ \boldsymbol{J}_2 \\ \vdots \\ \boldsymbol{J}_{n_v} \end{bmatrix}. \quad \boldsymbol{J}_i = \begin{bmatrix} \boldsymbol{J}_{Bi} & \boldsymbol{J}_{Mi} \end{bmatrix} = \begin{bmatrix} \boldsymbol{J}_{BTi} & \boldsymbol{J}_{MTi} \\ \boldsymbol{J}_{BRi} & \boldsymbol{J}_{MRi} \end{bmatrix},$$

is a $6\times(6+n_v)$ matrix. $\boldsymbol{J}_{BTi} = \begin{bmatrix} \boldsymbol{E} & \tilde{\boldsymbol{r}}_{0i}^T \end{bmatrix}$, $\boldsymbol{J}_{BRi} = [0 \quad \boldsymbol{E}]$, both are 3×6 matrices; $\boldsymbol{J}_{MRi} = \begin{bmatrix} \boldsymbol{L}_{i1} \, {}^1\boldsymbol{Z}_1 & \boldsymbol{L}_{i2} \, {}^2\boldsymbol{Z}_2 & \cdots & \boldsymbol{L}_{in_v} \, {}^{n_v}\boldsymbol{Z}_{n_v} \end{bmatrix}$, $\boldsymbol{J}_{MTi} = \begin{bmatrix} \boldsymbol{L}_{i1} \, {}^1\boldsymbol{Z}_1 \times (\boldsymbol{r}_i - \boldsymbol{p}_1) & \boldsymbol{L}_{i2} \, {}^2\boldsymbol{Z}_2 \times (\boldsymbol{r}_i - \boldsymbol{p}_2) & \ldots & \boldsymbol{L}_{in_v} \, {}^{n_v}\boldsymbol{Z}_{n_v} \times (\boldsymbol{r}_i - \boldsymbol{p}_{n_v}) \end{bmatrix}$, both are $3\times n_v$ matrices.

B. Generalized Dynamics Model

Substitute (5) into the kinetic energy equation:

$$T = \frac{1}{2}\sum_{i=0}^{n_v} (\boldsymbol{\omega}_i^T \boldsymbol{I}_i \boldsymbol{\omega}_i + m_i \boldsymbol{v}_i^T \boldsymbol{v}_i) = \frac{1}{2}\dot{\boldsymbol{\Phi}}^T \boldsymbol{H}_{sys}\dot{\boldsymbol{\Phi}} \tag{6}$$

where $\boldsymbol{H}_{sys}$ is the $(n_v + 6)\times(n_v + 6)$ system generalized inertia matrix [14]:

$$\boldsymbol{H}_{sys}=\begin{bmatrix} M_a(\boldsymbol{E})_{3\times3} & M_a(\tilde{\boldsymbol{r}}_{0g}^T)_{3\times3} & (\boldsymbol{J}_{Tg})_{3\times n_v} \\ M_a(\tilde{\boldsymbol{r}}_{0g})_{3\times3} & (\boldsymbol{H}_{\omega})_{3\times3} & (\boldsymbol{H}_{\omega\phi})_{3\times n_v} \\ (\boldsymbol{J}_{Tg}^T)_{n_v\times3} & (\boldsymbol{H}_{\omega\phi}^T)_{n_v\times3} & (\boldsymbol{H}_{\phi})_{n_v\times n_v} \end{bmatrix} \quad (7)$$

In Eq. (7), M_a is the overall mass of the robot, $\boldsymbol{r}_{0g}=\boldsymbol{r}_g-\boldsymbol{r}_0$,

$\boldsymbol{H}_{\omega}=\boldsymbol{I}_0+\sum_{i=1}^{n_v}(\boldsymbol{I}_i+m_i\tilde{\boldsymbol{r}}_{0i}\tilde{\boldsymbol{r}}_{0i}^T)=\boldsymbol{I}_0+\sum_{i=1}^{n_v}(\boldsymbol{I}_i+m_i\tilde{\boldsymbol{r}}_{0i}^T\tilde{\boldsymbol{r}}_{0i})$,

$\boldsymbol{J}_{Tg}=\sum_{i=0}^{n_v}m_i\boldsymbol{J}_{MTi}$, $\boldsymbol{H}_{\phi}=\sum_{i=1}^{n_v}(\boldsymbol{J}_{MRi}^T\boldsymbol{I}_i\boldsymbol{J}_{MRi}+m_i\boldsymbol{J}_{MTi}^T\boldsymbol{J}_{MTi})$, and

$\boldsymbol{H}_{\omega\phi}=\sum_{i=1}^{n_v}(\boldsymbol{I}_i\boldsymbol{J}_{MRi}+m_i\tilde{\boldsymbol{r}}_{oi}\boldsymbol{J}_{MTi})$.

According to the Lagrange function:

$$\boldsymbol{F}_{sys}=\boldsymbol{H}_{sys}(\boldsymbol{\Phi})\ddot{\boldsymbol{\Phi}}_{sys}+\boldsymbol{C}(\boldsymbol{\Phi},\dot{\boldsymbol{\Phi}})\dot{\boldsymbol{\Phi}}+\boldsymbol{f}(\dot{\boldsymbol{\Phi}})+\boldsymbol{G}(\boldsymbol{\Phi}) \quad (8)$$

where $\boldsymbol{C}$ is an $(n_v+6)\times(n_v+6)$ stiffness matrix describing the Coriolis and centripetal effects, which are proportional to $\dot{q}_i^2$ and $\dot{q}_i\dot{q}_j$, respectively; $\boldsymbol{f}$ is an $(n_v+6)\times1$ matrix that describes viscous and coulomb friction (typically negligible in a rigid-body dynamics system); $\boldsymbol{G}$ is an $(n_v+6)\times1$ gyroscopic vector reflecting gravity loading; and $\boldsymbol{F}_{\text{sys}}$ is the vector of generalized forces:

$$\boldsymbol{F}_{sys}=\boldsymbol{N}+\boldsymbol{J}_{ae}{}^T\boldsymbol{N}_{ae} \quad (9)$$

In Eq. (9), $\boldsymbol{N}$ is an $(n_v+6)\times1$ matrix including the forces ($\boldsymbol{F}_0$) and moments ($\boldsymbol{M}_0$) acting on the body, and those acting on the joints ($\boldsymbol{\tau}=[\tau_1 \quad \tau_2 \quad \cdots \quad \tau_{n_v}]^T$); $\boldsymbol{N}_{ae}$ is a $6n_w\times1$ vector including the external forces ($\boldsymbol{F}_e$) and moments ($\boldsymbol{M}_e$) from the soil that act on the wheel:

$$\boldsymbol{N}=\begin{bmatrix}\boldsymbol{F}_0\\ \boldsymbol{M}_0\\ \boldsymbol{\tau}\end{bmatrix},\ \boldsymbol{N}_{ae}=[\boldsymbol{F}_e^T(1)\ \ \boldsymbol{M}_e^T(1)\ \ \cdots\ \ \boldsymbol{F}_e^T(n_w)\ \ \boldsymbol{M}_e^T(n_w)]^T$$

The dynamics equation of a wheeled mobile robot including the wheel-soil interaction terramechanics is:

$$\begin{aligned}&\boldsymbol{H}_{sys}(\boldsymbol{\Phi})\ddot{\boldsymbol{\Phi}}_{sys}+\boldsymbol{C}(\boldsymbol{\Phi},\dot{\boldsymbol{\Phi}})\dot{\boldsymbol{\Phi}}+\boldsymbol{f}(\dot{\boldsymbol{\Phi}})+\boldsymbol{G}(\boldsymbol{\Phi})-\\ &\boldsymbol{N}-\boldsymbol{J}_{ae}{}^T\boldsymbol{N}_{ae}=0\end{aligned} \quad (10)$$

Let $\boldsymbol{C}(\boldsymbol{\Phi},\dot{\boldsymbol{\Phi}})\dot{\boldsymbol{\Phi}}+\boldsymbol{f}(\dot{\boldsymbol{\Phi}})+\boldsymbol{G}(\boldsymbol{\Phi})=\boldsymbol{D}$, so the generalized accelerations can be calculated according to Eq. (11):

$$\ddot{\boldsymbol{\Phi}}_{sys}=\boldsymbol{H}_{sys}^{-1}(\boldsymbol{N}+\boldsymbol{J}_{ae}{}^T\boldsymbol{N}_{ae}-\boldsymbol{D}) \quad (11)$$

Recursive Newton-Euler method is used to deduce an equation equivalent to Eq. (10) to calculate the unknown $\boldsymbol{D}$.

The Newton-Euler equations are:

$$\begin{cases}\boldsymbol{F}_i=m_i\dot{\boldsymbol{v}}_i\\ \boldsymbol{N}_i=\boldsymbol{I}_i\dot{\boldsymbol{\omega}}_i+\boldsymbol{\omega}_i\times\boldsymbol{I}_i\boldsymbol{\omega}_i\end{cases} \quad (12)$$

According to D'Alembert's principle, $\boldsymbol{f}_i$ and $\boldsymbol{m}_i$ impact on link i through joint i is:

$$\begin{cases}\boldsymbol{m}_i=\boldsymbol{M}_i+\sum_{j=i+1}^{n}\boldsymbol{S}_{ij}(\boldsymbol{l}_{ij}\times\boldsymbol{f}_j+\boldsymbol{m}_j)-\boldsymbol{S}_{ii}\times\\ \quad[\lambda_P(i)\boldsymbol{A}_i{}^i\boldsymbol{Z}_iq_i-\boldsymbol{c}_{ii}]\times(\boldsymbol{F}_i-m_i\boldsymbol{g})-\boldsymbol{S}_{ei}(\boldsymbol{l}_{ie}\times\boldsymbol{F}_{ei}+\boldsymbol{M}_{ei})\\ \boldsymbol{f}_i=\boldsymbol{F}_i-m_i\boldsymbol{g}+\sum_{j=i+1}^{n}\boldsymbol{S}_{ij}\boldsymbol{f}_j-\boldsymbol{S}_{ei}\boldsymbol{F}_{ei}\end{cases} \quad (13)$$

where $\lambda_P(i)$ is 1 for a prismatic joint and 0 for a rotational joint, $\boldsymbol{S}$ is the incidence matrix to find the upper connection of a link, and $\boldsymbol{S}_{ei}$ indicates whether i is an end point. The generalized force/moment of link i is:

$$\tau_i=\begin{cases}\boldsymbol{m}_i^T\boldsymbol{A}_i{}^i\boldsymbol{Z}_i & \text{(Rotational joint)}\\ \boldsymbol{f}_i^T\boldsymbol{A}_i{}^i\boldsymbol{Z}_i & \text{(Prismatic joint)}\end{cases} \quad (14)$$

The forces and moments that act on the body are:

$$\begin{cases}\boldsymbol{F}_0=\sum_{j=1}^{n}\boldsymbol{S}_{0j}\boldsymbol{f}_j+m_0(\dot{\boldsymbol{v}}_0-\boldsymbol{g})\\ \boldsymbol{M}_0=\sum_{j=1}^{n}\boldsymbol{S}_{0j}(\boldsymbol{c}_{0j}\times\boldsymbol{f}_j+\boldsymbol{m}_j)+\boldsymbol{I}_0\dot{\boldsymbol{\omega}}_0+\boldsymbol{\omega}_0\times\boldsymbol{I}_0\boldsymbol{\omega}_0\end{cases} \quad (15)$$

where $\boldsymbol{S}_{0j}$ is a flag vector to indicate whether j has a connection with the body.

According to Eq. (10), let the accelerations of all the generalized coordinates and the external forces/moments be zero; it is then possible to obtain $\boldsymbol{D}$ with Eqs. (14) and (15).

III. Wheel-soil interaction Terramechanics Models

The soil applies three forces and three moments to each wheel, as shown in Fig. 4. The normal force F_N can sustain the wheel. The cohesion and the shearing of the soil can generate a resistance moment M_R and a tractive force; the resistance force is caused by wheel sinking into the soil; the composition of the tractive and resistance forces is called drawbar pull F_{DP}, which is the effective force of driving a wheel. As a wheel steers or when a slip angle exists, there will be a side force F_S, a steering resistance moment M_S, and an overturning moment M_O acting on the wheel.

A. Driving model

Fig. 2 shows the diagram of lugged wheel-soil interaction mechanics, where z is wheel sinkage; θ_1, the entrance angle at which the wheel begins to contact the soil; θ_2, the exit angle at which the wheel loses contact with the soil; θ_m, the angle of maximum stress; θ_1', the angle where the soil starts to deform; W, the vertical load of the wheel; DP, the resistance force acting on the wheel; T, the driving torque of the motor; r, the wheel radius; h, the height of the lugs; v, the vehicle velocity; and ω, the angular velocity of the wheel. The soil interacts with the wheel in the form of continuous normal stress σ and shearing stress τ, which could be integrated to calculate the interaction mechanics. In order to improve the simulation speed, a simplified closed-form formula [15] is adopted and improved considering the effect of normal force, as given by Eq. (16).

$$\begin{cases}F_{DP}=[\frac{M_R(A^2+B^2)}{r_sAC}-\frac{BF_N}{A}](1+c_{P1}+c_{P2}s)(1+c_{P3}\frac{\overline{W}-F_N}{\overline{W}})\\ F_N=rbA\sigma_m+r_sbB\tau_m\\ M_R=\frac{r_s^2CD[bc+[1+c_M(\overline{W}-F_N)/\overline{W}]F_N\tan\varphi/(rA)]}{1+r_sBD\tan\varphi/(rA)}\end{cases} \quad (16)$$

In Eq. (16), s is the slip ratio defined in Ref. [16]; c_{P1} and c_{P2} are adopted to reflect the influence of the slip ratio on drawbar pull, then θ_m can be simplified as a half of θ_1; c_{P3} and c_M are parameters that compensate for the effect of normal force; $\overline{W}$ is the average normal force of the wheels; and

$\sigma_m=K_sr^N(\cos\theta_m-\cos\theta_1)^N$, $C=(\theta_1-\theta_2)/2$,

$$A = (\cos\theta_m - \cos\theta_2)/(\theta_m - \theta_2) + (\cos\theta_m - \cos\theta_1)/(\theta_1 - \theta_m),$$
$$B = (\sin\theta_m - \sin\theta_2)/(\theta_m - \theta_2) + (\sin\theta_m - \sin\theta_1)/(\theta_1 - \theta_m),$$
$$\tau_m = (c + \sigma_m \tan\phi) \times (1 - \exp\{-r_s[(\theta_1' - \theta_m) - (1-s)(\sin\theta_1' - \sin\theta_m)]/k\}).$$

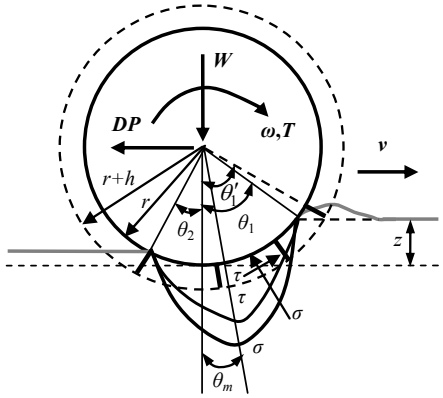

Fig.2 Lugged wheel-soil interaction mechanics diagram

The newly introduced parameters are:
$\theta_1' = \text{acos}[(r-z)/R_j]$, $K_s = k_c/b + k_\varphi$, $N = n_0 + n_1 s$, $\theta_2 \approx 0$.
The radius R_j is a value between r and r+h that compensates for the lug effect [16]. The soil parameters in the equations are: k_c, cohesive modulus; k_φ, frictional modulus; N, an improved soil sinkage exponent; c, cohesion of the soil; φ, the internal friction angle; and k, the shearing deformation modulus. n_0 and n_1 are coefficients for calculating N, which are important when predicting the slip-sinkage of wheels.

B. Steering Model

The model for calculating side force F_S is introduced in Ref. [11]:

$$F_S = rb\int_{\theta_2}^{\theta_1} \tau_y(\theta)d\theta + \int_{\theta_2}^{\theta_1} R_b(r - h(\theta)\cos\theta)d\theta \quad (17)$$

$$\tau_y(\theta) = [c + \sigma(\theta)]\{1 - \exp[-r(1-s)(\theta_1 - \theta)\tan\beta / k_y]\} \quad (18)$$

$$R_b = \cot X_c + \tan(X_c + \phi)\left\{hc + \frac{1}{2}\rho h^2\left[(\cot X_c + \frac{\cot X_c^{\,2}}{\cot\phi}\right]\right\} \quad (19)$$

where $X_c = \pi/4 - \varphi/2$; k_y is the shearing deformation modulus in the y direction; β is the skid angle; and h is the wheel height in the soil.

The overturning moment is approximated by Eq. (20):

$$M_O \approx F_S r \quad (20)$$

The steering resistance moment M_s is considered to be zero, and the motion of steering is simulated by kinematics method, as the steering torque has little influence on the motion of the entire rover, and the model is still under development.

IV. Deformable Rough Terrain Geometry Modeling

A. Contact Area Calculation

For simplification purposes, literature often assumes that the wheel soil interaction occurs at a single point, which may cause large errors when the robot moves in deformable rough terrain, and even result in simulation failure because of the abrupt changes in wheel sinkage and other forces. Calculating the interaction area of a wheel moving on soft soil is important for high-fidelity simulation, based on which, the interaction mechanics can be predicted and transformed.

Fig. 3 shows the interaction area of a wheel moving on rough terrain. The known parameters are: (x_w, y_w, z_w), the position of a wheel's center W; φ_w, the yaw angle of a wheel; and the Digital Evaluation Map (DEM) of the terrain. The interaction area is simplified as an inclined plane determined by points P_1, P_2, and P_3, the normal vector of which is:

$$\boldsymbol{z_e} = \begin{bmatrix} A_t \\ B_t \\ C_t \end{bmatrix} = \begin{bmatrix} x_2 - x_1 \\ y_2 - y_1 \\ z_2 - z_1 \end{bmatrix} \times \begin{bmatrix} x_3 - x_1 \\ y_3 - y_1 \\ z_3 - z_1 \end{bmatrix} \quad (21)$$

The equation of the inclined plane $P_1P_2P_3$ is therefore:

$$A_t(x - x_1) + B_t(y - y_1) + C_t(z - z_1) = 0. \quad (22)$$

P, the foot of perpendicular from point w to plane $P_1P_2P_3$, is located on line $(x - x_w)/A_t = (y - y_w)/B_t = (z - z_w)/C_t$. The coordinates of point E can be solved by substituting the line equation into Eq. (22). The length of wP is deduced:

$$\overline{wP} = \frac{|A_t(x_w - x_1) + B_t(y_w - y_1) + C_t(z_w - z_1)|}{\sqrt{A_t^2 + B_t^2 + C_t^2}} \quad (23)$$

The wheel sinkage is then determined by Eq. (24):

$$z = \overline{Pe} = r - \overline{wP} \quad (24)$$

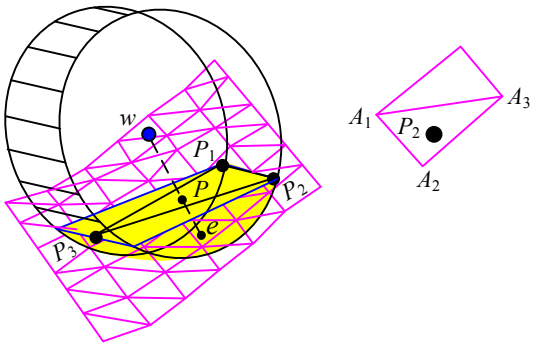

Fig. 3 Interaction area of a wheel moving on deformable rough terrain

Point P_2 is used to illustrate how to get the coordinates of points P_1, P_2, and P_3. A wheel moving on a random plane can be decomposed into climbing up/down a slope with an angle of θ_{cl} and traversing across a slope with an inclination angle of θ_{cr}, as shown in Fig. 4. Then, the x and y coordinates of point P_2 are:

$$\begin{cases} x_{P2} = x_w + r\cos\theta_{cr} \\ y_{P2} = y_w + r\sin\theta_1\cos\theta_{cl} \end{cases} \quad (25)$$

The coordinates of points A_1, A_2, and A_3 are easy to find by referring to the DEM. z_{P2} can then be determined using the same method as that for calculating point E.

B. Terminal Force Transformation Matrix

Fig. 4 shows the forces and moments that act on the wheel by the soil. $\{\Sigma_e\}$ and $\{\Sigma_w\}$ are coordinate systems with the same orientation and different origins, at the end point and wheel center, respectively.

$\boldsymbol{x}_e$ is the intersection line between the wheel-soil interaction plane and the plane with an included angle of φ_w between the x axis: $x\tan\varphi_w - y + D' = 0$. It is deduced that:

$$\boldsymbol{x_e} = \{C_t, C_t \tan\varphi_w, -A_t - B_t \tan\varphi_w\} \quad (26)$$

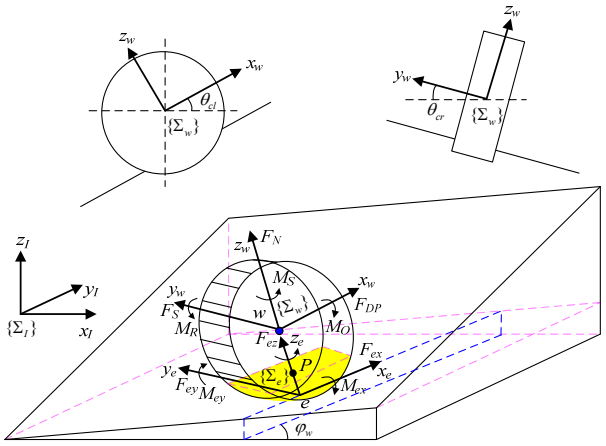

Fig.4 Force analysis of a wheel moving on a random slope

Then, the vector direction of y_e is:

$$\boldsymbol{y_e} = \boldsymbol{z_e} \times \boldsymbol{x_e} = \begin{bmatrix} -A_t B_t - (B_t^2 + C_t^2)\tan\varphi_w \\ C_t^2 + A_t(A_t + B_t \tan\varphi_w) \\ A_t C_t \tan\varphi_w - B_t C_t \end{bmatrix} \quad (27)$$

θ_{cl} (θ_{cr}) is the angle between $\boldsymbol{x}_e$ ($\boldsymbol{y}_e$) and the horizontal plane, which can be calculated by:

$$\begin{cases} \theta_{cl} = \arcsin[(-A_t - B_t \tan\varphi_w)/X_1] \\ \theta_{cr} = \arcsin[C_t(A_t \tan\varphi_w - B_t)/X_2] \end{cases} \quad (28)$$

where $X_1 = \sqrt{C_t^2(1+\tan^2\varphi_w) + (A_t + B_t\tan\varphi_w)^2}$,

$X_2 = \sqrt{X_3[A_t^2 + C_t^2 + 2A_tB_t\tan\varphi_w + (B_t^2 + C_t^2)\tan^2\varphi_w]}$,

$X_3 = \sqrt{A_t^2 + B_t^2 + C_t^2}$. According to $\boldsymbol{x}_e$, $\boldsymbol{y}_e$, and $\boldsymbol{z}_e$, the transformation matrix from $\{\Sigma_e\}$to $\{\Sigma_I\}$ is:

$$\boldsymbol{A_e} = \begin{bmatrix} \frac{C_t}{X_1} & \frac{-A_tB_t - (B_t^2+C_t^2)\tan\varphi_w}{X_2} & \frac{A_t}{X_3} \\ \frac{C_t\tan\varphi_w}{X_1} & \frac{C_t^2 + A_t^2 + A_tB_t\tan\varphi_w}{X_2} & \frac{B_t}{X_3} \\ \frac{-A_t - B_t\tan\varphi_w}{X_1} & \frac{A_tC_t\tan\varphi_w - B_tC_t}{X_2} & \frac{C_t}{X_3} \end{bmatrix} \quad (29)$$

The external forces and torques that act on the wheel-soil interaction point are:

$$\begin{cases} {}^e\boldsymbol{F}_e = {}^w\boldsymbol{F}_e = [F_{DP} \quad F_S \quad F_N]^T \\ {}^e\boldsymbol{M}_e = [M_O - rF_S \quad -M_R + rF_{DP} \quad M_S]^T \end{cases} \quad (30)$$

The equivalent forces and moments that act on the wheel in the inertial coordinate $\{\Sigma_I\}$ are:

$$\begin{cases} \boldsymbol{F}_e = \boldsymbol{A}_e\, {}^e\boldsymbol{F}_e \\ \boldsymbol{M}_e = \boldsymbol{A}_e\, {}^e\boldsymbol{M}_e \end{cases} \quad (31)$$

V. Implementation, Validation, and Example

A. Simulation Implementation

The numerical simulation program was developed based on a Matlab toolbox called SpaceDyn [14]. The principle diagram is shown in Fig. 5. Given DEM terrain, soil parameters, and rover model parameters, the program calculates the wheel-soil interaction area, predicts the external forces that act on the wheel, calculates the accelerations of the generalized coordinates based on the dynamics model, and then integrates them to obtain their velocities and positions based on the kinematics equations.

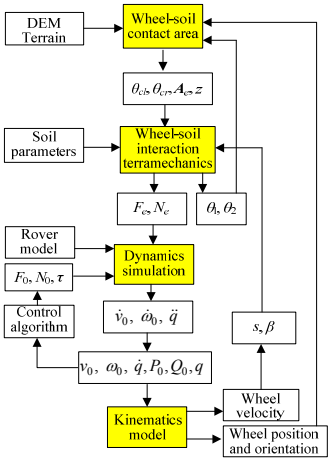

Fig. 5 Principle diagram of dynamics simulation

B. Experimental Validation

El-Dorado II, a four-wheeled mobile robot developed at SRL was used for validating the simulation. The robot has four F/T sensors to measure the wheel-soil interaction terramechanics. Based on a telecentric camera, a visual odometry system was developed to measure the position of the rover body and the slip ratio of the wheels. The wheel entrance angles used for calculating the wheel sinkage were measured with an angle meter. Two groups of experiments were performed. In group 1, resistance forces were applied to the rover with counterweights from 0N to 60N, with a step of 10N, to generate different slip ratios. In group 2, the rover was controlled to climb up slopes ranging from 0° to 15°, with a step of 3°, as shown in Fig. 6.

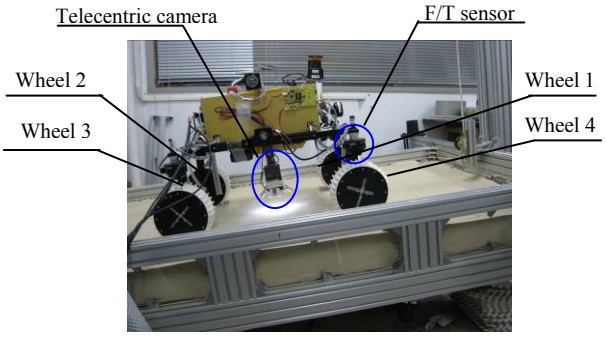

Fig. 6 Slope-climbing experiment using El-Dorado II robot

The parameters of the Toyoura soft sand are identified from the experimental data: K_s = 1796 Kpa/m^N, c = 24.5 Pa, φ = 35.75°, K = 10.45 mm. k_y is 19 mm according to [12]. When the robot climbs up slopes, the remaining parameters are: n_0 = 0.66, n_1 = 0.72, c_{P1} = -0.379, c_{P2} = 0.616, c_{P3} = -0.448, C_M = 0.214; on flat terrain the parameters are n_0 = 0.63, n_1 = 0.72, c_{P1} = -0.276, c_{P2} = 0.633, c_{P3} = -0.304, C_M = 0.354.

Comparisons of the simulation and experimental results are shown in Figs. 7 and 8. Not only can the motion of the robot be predicted with high-fidelity, as indicated by the slip ratio,

so too can the drawbar pull, moment of resistance, as well as the normal force and wheel sinkage.

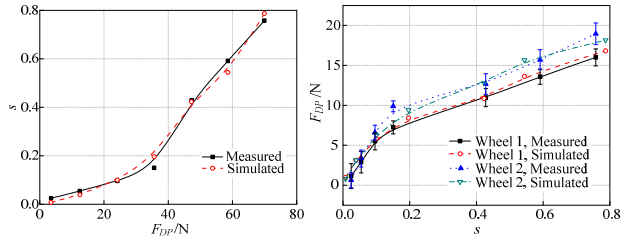

Fig. 7 Simulation and experimental results for robot moving on flat terrain

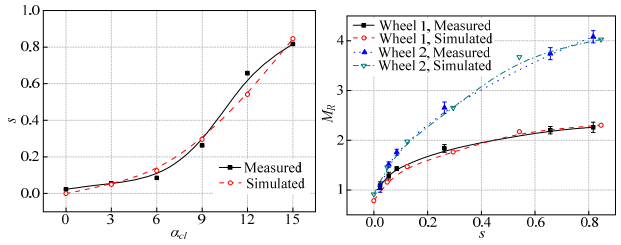

Fig. 8 Simulation and experimental results for robot climbing up slopes

C. *Simulation on Deformable Rough Terrain*

The robot was controlled to move from (0.5 m, 0.5 m) to (5 m, 5 m) on the randomly generated rough terrain shown in Fig. 9, with an initial yaw angle of 45°. While moving, the robot deviates from the scheduled path because of the inclination angle of the terrain. Fig. 10 shows the slope angles that wheel number 4 traversed over, the RPY (raw, pitch and yaw) angles of the body and q_1, q_2 joint angles ($q_1 = -q_2$), the slip ratios and normal forces.

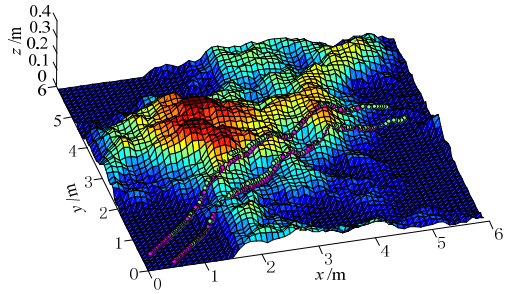

Fig. 9 Rough terrain and wheel trajectories

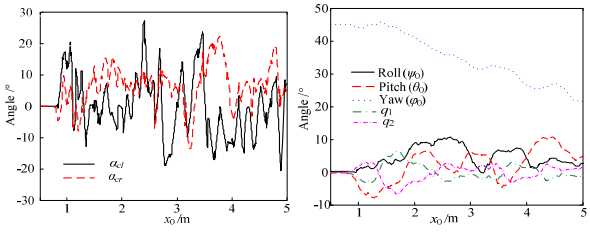

(a) Slope angles for wheel 4 (b) RPY, q_1 and q_2 angles

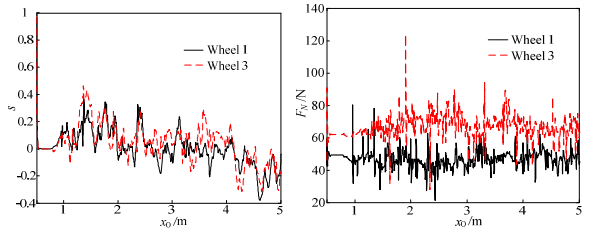

(c) Slip ratios (d) Normal forces

Fig. 10 Simulation results for El-Dorado II moving on deformable rough terrain

VI. Conclusion and Future Work

The models for dynamics, wheel-soil interaction terramechanics and deformable rough terrain presented in this paper effectively, and with reasonable precision, simulate the motion of a robot moving on deformable rough terrain. The experiments provide verification.

Future work should include the development of a skid model and a steering model, validation of the simulation results on rough terrain, and the application to a robot in terms of design parameter optimization and control algorithm verification.

References

[1] L. Ding, H. Gao, Z. Deng, et al., "Design of comprehensive high-fidelity/high-speed virtual simulation system for lunar rover," in *Proc. 2008 IEEE Int. Conf. on Robotics, Automation and Mechatronics*, Chengdu, China, 2008: 1118–1123.

[2] J. Yen, A. Jain, and J. (Bob) Balaram, "ROAMS: rover analysis modeling and simulation software," in *Proc. 5th i-SAIRAS,* Noordwijk, Netherlands, 1999.

[3] A. Jain, J. (Bob) Balaram, J. Cameron, et al., "Recent developments in the ROAMS planetary rover simulation environment," in *Proc. IEEE Aerospace Conference Proceedings*, 2004: 861–875.

[4] G. SohL, and A. Jain, "Wheel-terrain contact modeling in the ROAMS planetary rover simulation," in *Proc. IDETC'05 ASME Int. Design Engineering Technical Conf. and Computers and Information in Engineering Conf.*, Long Beach, CA, 2005.

[5] D. S. Apostolopoulos, "Analytical configuration of wheeled robotics locomotion," *The Robotics Institute of Carnegie Mellon University Technical Report CMU-RI-TR-01-08*, 2001.

[6] S. Michaud, L. Richter, N. Patel, et al., "RCET: rover chassis evaluation tools," in *Proc. 8th ESA Workshop on ASTRA*, ESTEC, Noordwijk, Netherlands, 2004.

[7] N. Patel, A. Ellery, E. Allouis, et al., "Rover mobility performance evaluation tool (RMPET): a systematic tool for rover chassis evaluation via application of Bekker theory," in *Proc. 8th ESA Workshop on Advanced Space Technologies for Robotics and Automation*, ESTEC, Noordwijk, The Netherlands, 2004: 251–258.

[8] R. Bauer, W. Leung and T. Barfoot, "Development of a dynamic simulation tool for the Exomars rover," in *Proc. 8th i-SAIRAS*, Munich, Germany, 2005.

[9] http://www.astro.mech.tohoku.ac.jp/~ishigami/rover/.

[10] K. Yoshida, T. Watanabe, et al., "Terramechanics-based analysis and traction control of a lunar/planetary rover," in *Proc. 4th Int. Conf. on Field and Service Robotics*, Lake Yamanaka, Japan, 2003: 225–234.

[11] K. Yoshida and G. Ishigami, "Steering characteristics of a rigid wheel for exploration on loose soil," in *Proc. 2004 IEEE Int. Conf. on Intelligent Robots and Systems*, Sendai, Japan, 2004: 3995–4000.

[12] G. ISHIGAMI, "Terramechanics-based analysis and control for lunar/planetary exploration robots," Ph.D. dissertation, Tohoku University, Sendai, 2008.

[13] G. Ishigami, K. Nagatani and K. Yoshida, "Path planning for planetary exploration rovers and its evaluation based on wheel slip dynamics," in *Proc. IEEE ICRA.*, Roma, Italy, 2007: 2361–2366.

[14] Kazuya Yoshida, "The SpaceDyn: a MATLAB Toolbox for Space and Mobile Robots," Journal of Robotics and Mechatronics, 12 (4): 411–416.

[15] L. Ding, K. Yoshida, K. Nagatani, H. Gao, and Z. Deng, "Parameter Identification for Planetary Soil Based on Decoupled Analytical Wheel-Soil Interaction Terramechanics Model," in *Proc. 2009 IEEE/RSJ Int. Conf. Intelligent Robots and Systems*, St. Louis, MO, 2009: 4122-4127.

[16] L. Ding, H. Gao, Z. Deng, K. Yoshida and K. Nagatani, "Slip ratio for lugged wheel of planetary rover in deformable soil: definition and estimation," in *Proc. IEEE/RSJ Int. Conf. Intelligent Robots and Systems*, St. Louis, MO, 2009: 3343-3348.